Amin Soltani, An Deng, Abbas Taheri

Swell-compression characteristics of a fiber-reinforced expansive soil

Geotextiles and Geomembranes, 2018; 46(2):183-189

Published at: http://dx.doi.org/10.1016/j.geotexmem.2017.11.009

Swell-Compression Characteristics of a Fiber-Reinforced Expansive Soil: Experiments and Modelling

Amin Soltani[1*], An Deng[2] and Abbas Taheri[3]

[1] PhD Student, *School of Civil, Environmental and Mining Engineering, The University of Adelaide, Adelaide, SA 5005, Australia* (**[*]Corresponding author)**
Tel: +61-8-83132830
Fax: +61-8-83134359
Email: Amin.Soltani@adelaide.edu.au

[2] Senior Lecturer, *School of Civil, Environmental and Mining Engineering, The University of Adelaide, Adelaide, SA 5005, Australia*
Tel: +61-8-83132830
Fax: +61-8-83134359
Email: An.Deng@adelaide.edu.au

[3] Senior Lecturer, *School of Civil, Environmental and Mining Engineering, The University of Adelaide, Adelaide, SA 5005, Australia*
Tel: +61-8-83130906
Fax: +61-8-83134359
Email: Abbas.Taheri@adelaide.edu.au

Swell-Compression Characteristics of a Fiber-Reinforced Expansive Soil: Experiments and Modelling

Abstract

This study presents results of an experimental program in respect to fiber's capacity of mitigating the swelling behavior of an expansive soil. Two types of tape-shaped synthetic fibers, i.e. fiber A (width f_w=2.5mm) and fiber B (f_w=7mm) were used as the reinforcements. Fibers were incorporated at three contents, i.e. f_c=0.5%, 1% and 1.5%, each having two aspect ratios (i.e. f_{AR}=15/2.5 and 30/2.5 for fiber A, and f_{AR}=15/7 and 30/7 for fiber B). Samples were prepared at optimum moisture content and maximum dry unit weight, and were further subjected to oedometer swell-compression tests. An in-depth discussion on the swell-time and compression-stress characteristics was also presented. For a given type of included fiber, reduction in swelling potential and swelling pressure was observed to be a direct function of f_c and f_{AR}, with the former taking on a more pronounced role. Furthermore, for a given fiber content and fiber length, the greater fiber width (lower f_{AR}) assumed more efficiency in restricting swelling. The hyperbola concept was extended to the swell-compression framework, promoting simple equations capable of simulating the swell-compression behavior of the fiber-reinforced soil with an acceptable degree of accuracy.

Keywords: Expansive soil; Tape-shaped fibers; Aspect ratio; Swelling potential; Swelling pressure; Hyperbola concept.

Notations

C_c	Compression index
C_{ps}	Primary swelling rate
C_{ss}	Secondary swelling rate
e_0	Initial void ratio
f_{AR}	Fiber aspect ratio (fiber length to width ratio)
f_c	Fiber content
f_l	Fiber length
f_{TS}	Fiber tensile strength
f_w	Fiber width
NRMSE	Normalized root mean square error
P_s	Swelling pressure
R^2	Coefficient of determination
S_p	Swelling potential
t	Elapsed time of swelling
t_{is}	Completion time of the initial swelling phase
t_{ps}	Completion time of the primary swelling phase
t_{ss}	Completion time of the secondary swelling phase
$1/\beta_s$	Long-term predicted swelling potential
ε_a	Axial strain (swelling or compression)
ε_{ais}	Initial swelling strain
ε_{aps}	Primary swelling strain
ε_{ass}	Secondary swelling strain
σ'	Effective stress
σ'_0	Nominal overburden stress during swelling
σ_y	Yield stress

1. Introduction

As a consequence of their inherent characteristics including low strength, high compressibility and a high potential for swelling and shrinkage, expansive soils are often characterized as unsuitable construction materials for the majority of civil engineering applications (Nalbantoglu 2006). Therefore, such soils often require modification – a process commonly referred to as stabilization – to satisfy design criteria prior application. Stabilization may be achieved through two approaches, i.e. chemical and mechanical techniques. Chemical techniques mainly include the addition of chemical agents (e.g. lime, cement and polymer binder) to the soil mass, enhancing physico-chemical interactions and thereby amending the soil fabric into a coherent matrix of improved properties (e.g. Al-Rawas et al. 2005; Mirzababaei et al. 2009; Yazdandoust and Yasrobi 2010; Kalkan 2011; Estabragh et al. 2014). The mechanical approach makes use of mechanical effort (e.g. compaction) with the aid of reinforcements. Common reinforcements include fibers of synthetic (e.g. polypropylene and nylon) and natural (e.g. coir and palm) origin or other fiber-like materials such as plastic waste strips, shredded tires and waste carpet fibers. As the global community is shifting towards a more sustainable mindset, alternatives capable of replacing or minimizing the use of traditional cementitious agents have been highly encouraged. The use of fibers may be regarded among the most well-received propositions in this context.

The fiber assemblage randomly distributes in the soil regime, and where optimized in dosage and geometry, amends the expansive soil in respect to moisture insensitivity (i.e. swell-shrink related volume changes), strength increase, and ductility improvement (e.g. Puppala and Musenda 2000; Tang et al. 2007; Abdi et al. 2008; Al-Akhras et al. 2008; Sivakumar Babu et al. 2008; Attom et al. 2009; Viswanadham et al. 2009[a, b]; Tang et al. 2010; Plé and Lê 2012; Trouzine et al. 2012; Mirzababaei et al. 2013; Estabragh et al. 2014; Phanikumar and Singla 2016; Chaduvula et al. 2017). In some cases, a combination of fibers and traditional cementitious agents may be required to address sever expansive potential (e.g. Cai et al. 2006; Punthutaecha et al. 2006; Kumar et al. 2007; Shahbazi et al. 2016). Based on these studies, improvement in strength or swelling characteristics have been primarily reported as a function of fiber content. However, fiber geometrical properties, mainly defined in terms of aspect ratio (fiber length to the diameter or width ratio), also portrays an equally important role in yielding an effective stabilization scheme.

Some of the more recent contributions addressing the aspect ratio-dependent swelling phenomenon have been provided in Table 1. A rather common emphasis on the application of bar-shaped fibers with relatively small diameters, yielding relatively large aspect ratios may be observed among the documented studies. Such materials when applied at high contents are prone to clustering, thus would be associated with implementation difficulties under filed conditions. Meanwhile, tape-shaped fibers with relatively large widths, promoting relatively small aspect ratios have been less regarded in the literature. Such materials are mainly consumed in the packaging industry and are available in abundance, posing a problem for safe disposal without degrading the environment. As such, its beneficial reuse as an alternative to bar-shaped fibers may provide a more feasible stabilization scheme. To address any remaining ambiguities associated with adopting appropriate aspect ratios, this study intends to evaluate the effect of other less adopted aspect ratio values on the swell-compressibility characteristics of a highly expansive soil through a series of oedometer swell-compression tests. In addition, the hyperbola concept was extended to the swell-compression framework, resulting in simple equations capable of simulating the swell-compression behavior of fiber-reinforced expansive soils.

2. Materials and methods

2.1. *Soil*

The soil used in this study was clay of high plasticity (CH). X-ray diffraction (XRD) analysis identified the minerals of quartz, calcite, Na/Ca-feldspar, K-feldspar, and clay minerals group of illite and montmorillonite. Other soil properties included a pH of 8.3, electrical conductivity (EC) of 10.25dS/m and cation exchange capacity (CEC) of 17.95meq/100gr. Typical mechanical properties, determined as per relevant ASTM standards, are provided in Table 2. The swelling potential (i.e. S_p^{7kpa}) and swelling pressure were 17.50% and 325kPa, respectively; from which the soil was graded into *highly expansive* in accordance with the Sridharan and Prakash (2000) classification criteria.

2.2. *Fibers*

Two types of tape-shaped polypropylene fibers, i.e. fiber A (width f_w=2.5mm) and fiber B (f_w=7mm) as illustrated in Fig. 1, were used as the reinforcements. Both fibers were cut into two lengths, i.e. f_l=15mm and 30mm, ending up with aspect ratios of f_{AR}=15/2.5 and 30/2.5 for fiber A, and f_{AR}=15/7 and 30/7 for fiber B. Each of the four fiber choices was included into the soil at three contents, i.e. f_c=0.5%, 1% and 1.5%. Physical and mechanical properties of the fibers, as supplied by the manufacturer, are presented in Table 3.

2.3. *Sample preparation*

A series of standard compaction tests were carried out on natural soil and various soil-fiber mixtures in accordance with the ASTM D698 standard. The mixtures and corresponding compaction results are provided in Table 4. Minor variations were observed for optimum moisture content, while the maximum dry unit weight displayed a marginal decreasing trend with increase in fiber content, mainly attributed to the lower specific gravity and larger specific surface area of fibers compared to soil particles (Estabragh et al. 2012; Kalkan 2013; Estabragh et al. 2014). Samples were prepared by static compaction at corresponding optimum moisture content and maximum dry unit weight values (see Table 4). The required amount of water corresponding to the desired optimum moisture content was added to each mixture, and manually mixed as conducted in Tang et al. (2007), Consoli et al. (2009) and Estabragh et al. (2014, 2016). Extensive care was dedicated to pulverize the lumped particles, targeting homogeneity of mixtures. Mixtures were then enclosed in plastic bags and stored under room temperature conditions for 24 hours, ensuring even distribution of moisture throughout the soil mass. A special split mold was designed and fabricated from stainless steel to accomplish static compaction. The mold consisted of three sections, i.e. the top collar, the middle oedometer ring, and the bottom collar. The oedometer ring measures 75mm in diameter and 20mm in height and accommodates the sample for the swell-compression test. The inner surface of the mold was smeared with a thin layer of silicon grease to avoid friction during compaction. Mixtures were compressed in the mold at three layers by a constant displacement rate of 1.5mm/min to a specific compaction load, each layer having attained the desired maximum dry unit weight. The required compaction load was different for each mixture and was obtained through trial and error. The surface of the first and second compacted layers were scarified to ensure a good bond between adjacent layers of the mixture.

2.4. *Swell-compression test*

Samples were subjected to the one-dimensional oedometer swell-compression test as specified in the ASTM D4546 standard. The test included two stages, i.e. swell and compression. In the first stage, the desired sample was allowed to freely swell under a low nominal overburden stress of σ'_0 =1kPa. The incurred axial swelling strain was recorded during various swelling time intervals to a point in which swell-time equilibrium, a state corresponding to the swelling potential of the sample, S_p, was achieved. During compression, the swollen sample was gradually loaded to arrest the built-up axial swelling strain. The stress required to retain the initial placement or void ratio of the sample was taken as the swelling pressure P_s (Sridharan et al. 1986).

3. Results and discussion

Axial strain-time curves obtained from one-dimensional oedeometer swell tests are illustrated in Fig. 2 (2a: f_{AR}=15/2.5; 2b: f_{AR}=30/2.5) and Fig. 3 (3a: f_{AR}=15/7; 3b: f_{AR}=30/7) for fibers A and B, respectively. As a result of fiber-reinforcement, the axial strain-time locus experienced a major downward shift over the ε_a:log$t$ space, indicating a significant reduction in the magnitude of exhibited swelling strain and thus swelling potential during swell evolvement. At a specific elapsed time of swelling and for a given type of included fiber corresponding to a particular aspect ratio, an increase in fiber content f_c was accompanied by a significant reduction in swelling strain. At t=1440min, for instance, natural soil displayed an axial swelling strain of $\varepsilon_a(t)$=22.15%; while the inclusion of 0.5%, 1% and 1.5% fiber A (f_{AR}=15/2.5) led to $\varepsilon_a(t)$=14.90%, 12.05% and 10.05%, respectively (see Fig. 2a). A similar yet less pronounced case can also be made for fiber aspect ratio f_{AR}. At t=1440min, for instance, fiber B corresponding to f_c=1% and f_{AR}=15/7 resulted in $\varepsilon_a(t)$=9.97%; while for f_{AR}=30/7 of the same inclusion, $\varepsilon_a(t)$=8.15% was observed (compare Figs. 3a and 3b). Natural soil exhibited a swelling potential of S_p=26.40%. Maximum reduction in S_p was achieved in the case of f_c=1.5% corresponding to f_{AR}=30/2.5 and 30/7 for fibers A and B, respectively. These samples resulted in S_p=16.00% and 12.15%, respectively.

Axial strain-effective stress curves obtained from one-dimensional compression tests are illustrated in Fig. 4 (4a: f_{AR}=15/2.5; 4b: f_{AR}=30/2.5) and Fig. 5 (5a: f_{AR}=15/7; 5b: f_{AR}=30/7) for fibers A and B, respectively. Similarly, the inclusion of fibers to the soil mass altered the axial strain-effective stress locus, promoting a noticeable downward shift over the ε_a:logσ' space, and thus a significant reduction in swelling pressure. In general, reduction in swelling pressure P_s follows a trend similar to that of swelling potential S_p. For instance, the swelling pressure dropped from P_s=325kPa for natural soil to 215kPa for the sample reinforced with 0.5% fiber A corresponding to f_{AR}=15/2.5. The value further decreased to P_s=205kPa at f_{AR}=30/2.5, indicating an aspect ratio-dependent compressibility (compare Figs. 4a and 4b). Similar variations were also observed for the same inclusion of fiber B where P_s dropped from 201kPa at f_{AR}=15/7 to 158kPa at f_{AR}=30/7 (compare Figs. 5a and 5b). Similar to S_p, maximum reduction in P_s was achieved in the case of f_c=1.5% corresponding to

f_{AR}=30/2.5 and 30/7 for fibers A and B, respectively. These samples resulted in P_s=135kPa and 95kPa, respectively.

Figs. 6a and 6b illustrate the variations of swelling potential and swelling pressure against fiber content f_c for the tested samples. For a specific type of included fiber, reduction in S_p and P_s may be considered as a function of f_c and f_{AR}. The magnitude of decrease, however, seems to be dominated by f_c, while f_{AR} also portrays a significant yet less pronounced role. In addition, for a given fiber content and fiber length, a greater fiber width and thus lower aspect ratio (i.e. fiber B versus fiber A) assumes more efficiency in reducing the effect of swelling. The fiber inclusions are able to amend the soil fabric through improvement achieved in three aspects, i.e. resistive tension forces generated due to soil-fiber contact (Al-Akhras et al. 2008; Viswanadham et al. 2009[a]; Trouzine et al. 2012), soil-fiber interlock (Tang et al. 2007, 2010; Kalkan 2013; Phanikumar and Singla 2016), and fiber non-wetting attribute (Cai et al. 2006; Viswanadham et al. 2009[b]; Estabragh et al. 2014). Resistive tension forces grow as a consequence of fibers experiencing tensile stress in the presence of strong swelling forces. Increase in fiber content leads to an increase in total surface area, promoting a greater contact level between fibers and soil particles. This in turn increases the resistive tension forces among fibers, thus restricting the effect of swelling. Meanwhile, the randomly distributed fibers resemble a spatial three-dimensional network to weave or interlock soil particles into a coherent matrix of restricted heave. The greater the number of included fibers (increase in f_c) the more effective the interlocking effect. The swell dependence on aspect ratio is ascribed to the improvement mechanisms, i.e. resistive tension forces and interlocking. For a given type of included fiber, an increase in f_{AR} increases soil-fiber contacts, in turn generating a greater net resistive tension force among fibers coupled with an enhanced soil-fiber interlocking, restricting the effect of swelling. This improvement mechanism is in line with the fiber tensile strength f_{TS}, i.e. 3000MPa for fiber B and 1250MPa for fiber A (see Table 3). The more resilient the fiber to withstand stretching along its axis, the less chance the swelling forces may have to facilitate movement of soil particles interlocked to the fiber.

4. Swell-compression model

4.1. *Description*

As illustrated in Fig. 7a, the axial strain-time relationship plotted over the ε_a:log$t$ space develops into an *S*-shaped curve, graphically represented by the initial, primary and secondary swelling; phases during which swelling takes place (Dakshanamurthy 1978; Sivapullaiah et al. 1996; Sridharan and Gurtug 2004; Rao et al. 2006; Cui et al. 2012; Ye et al. 2015; Chen et al. 2017). The initial swelling phase, referred to as the first inter-layer or inter-crystalline swelling, involves macro-structural rearrangements, promoting small volume changes mainly less than 10% of the total volume increase. Inter-layer swelling continues into the primary swelling phase which constitutes for up to 80% of the total volume increase, and is graphically represented by a steep-sloped linear portion bounded by the initial and primary swelling time margins. The secondary swelling phase takes place as a result of double-layer repulsion, displaying small time-dependent volume changes. Both the primary and secondary swelling phases occur at micro-structural level where swelling of active clay minerals take place. Critical variables obtained from the *S*-shaped curve, defined by a conventional graphical construction as outlined in Fig. 7a, are regarded as useful concepts capable of predicting short- and long-term heave under field conditions (Sridharan and Gurtug 2004), which may be characterized as: **i**) completion time of the initial and primary swelling phases (t_{is} and t_{ps}); **ii**) initial, primary and secondary swelling strains (ε_{ais}, ε_{aps} and ε_{ass}); **iii**) primary and secondary swelling rates, C_{ps} and C_{ss}, defined as:

$$C_{ps} = \frac{(\%)\varepsilon_{aps}}{10^{-2} \times \log\left(\dfrac{t_{ps}}{t_{is}}\right)} \tag{1}$$

$$C_{ss} = \frac{(\%)\varepsilon_{ass}}{10^{-2} \times \log\left(\dfrac{t_{ss}}{t_{ps}}\right)} \tag{2}$$

Where t_{ss} is completion time of the secondary swelling phase.

A similar formulation occurs for the axial strain-effective stress relationship plotted over the ε_a:logσ' space, as illustrated in Fig. 7b. The curve can be divided into two regions, namely the elastic (recompression) and plastic (virgin compression) compression zones; phases during which compression takes place. The two regions are separated by the yield stress (σ'=σ_y), a transitional stress state which divides the compressibility of the soil into a region of small-elastic and large-plastic deformations (Casagrande 1936; Boone 2010). The yield stress σ_y was defined as the intersection of the recompression and virgin compression lines over the semi-log space of void ratio and effective stress (Cui and Delage 1996; Estabragh et al. 2011). Slope of the linear post-yield segment, depicted as VCL in Fig. 7b, over the ε_a:logσ' space may be adopted to represent the compression index (C_c) by:

$$C_c = \frac{(1+e_0)\overbrace{\Delta\varepsilon_a(\sigma')}^{(\%)}}{10^{-2} \times \log \Delta\sigma'} \tag{3}$$

Swell-time curve variables for the tested samples are provided in Table 5. As demonstrated in the table, t_{is} and t_{ps} varied in a way opposite to that of swelling potential S_p. The primary and secondary swelling strains mainly demonstrated a trend similar to that of S_p, meaning that for a given type of included fiber, f_c=1.5% corresponding to the greater aspect ratio (i.e. f_{AR}=30/2.5 for fiber A and f_{AR}=30/7 for fiber B) promoted the lowest ε_{aps} and ε_{ass} values. The initial swelling strain ε_{ais} for fiber-reinforced samples also exhibited a noticeable decrease compared to that of natural soil, however, no specific trend was observed. Variations of C_{ps} and C_{ss} with f_c for various reinforcement scenarios are, respectively, illustrated in Figs. 8a and 8b. The fiber inclusions led to a noticeable decrease in C_{ps} and C_{ss}, indicating a capacity of counteracting the heave in magnitude and time. The greater the fiber content or the wider the fiber the less the swelling rates, following a monotonic trend for the tested samples. As an optimal case, C_{ps} and C_{ss} decreased from 1.23×10^{-1} and 3.87×10^{-2} for natural soil to 6.52×10^{-2} and 1.99×10^{-2} for the sample reinforced with fiber B where f_c=1.5% and f_{AR}=30/7, respectively.

Variations of C_c and σ_y for the tested samples are provided in Table 5. Both C_c and σ_y are dependent on fiber content, demonstrating a fall-rise trend, unanimously decreasing at f_c=0.5% then rising for higher f_c inclusions.

As a result, C_c and σ_y nearly reverted to the initial value obtained for natural soil in some circumstances. Such a fall-rise relationship suggests that f_c=0.5% may be optimal in respect to reducing material collapse when stressed. Excessive fiber inclusions likely give rise to significant deformation. It is noteworthy to cross check the compression characteristics with the swelling rates which are in favor of a higher fiber content. This discrepancy implies that the fiber, like a net, is effective at weaving the soil into a coherent matrix of restricted heave, while when excessively included raises deformation concerns.

4.2 *Model development*

The rectangular hyperbola concept has been widely acknowledged as a simple yet accurate approach capable of reproducing the *S*-shaped swell-time curve over a wide time domain of $t\in(0,\infty)$ (Dakshanamurthy 1978; Sridharan et al. 1986; Sivapullaiah et al. 1996; Sridharan and Gurtug 2004; Ye et al. 2015; Soltani et al. 2017). The two-parameter rectangular hyperbola with respect to the axial strain-time relationship can be expressed as:

$$(\%)\varepsilon_a(t)=\frac{t}{\alpha_s+\beta_s t}$$
$$\text{Boundary conditions}:\begin{cases}\varepsilon_a(0)=0\\ \lim\limits_{t\to\infty}\left[\varepsilon_a(t)\right]\cong\dfrac{1}{\beta_s}\end{cases}\tag{4}$$

Where α_s and β_s are the fitting parameters, and $1/\beta_s$ defines the positive asymptotic value of the function when $t\to\infty$, equally the long-term predicted swelling potential.

Other forms of the hyperbola function have been adopted in the literature to represent the void ratio-effective stress relationship during compression (Sridharan and Gurtug 2005; Chong and Santamarina 2016; Soltani 2016):

$$e(\sigma')=e_0-\frac{\sigma'^{\mu}}{\alpha_c+\beta_c\sigma'^{\mu}}$$
$$\text{Boundary conditions}:\begin{cases}e(0)=e_0\\ \lim\limits_{\sigma'\to\infty}\left[e(\sigma')\right]\cong e_0-\dfrac{1}{\beta_c}\end{cases}\tag{5}$$

Where $e(\sigma')$ is void ratio in respect to effective stress σ', e_0 is the initial void ratio, and α_c, β_c and μ are the fitting parameters.

By setting $e(\sigma')\to\varepsilon_a(\sigma')$, $e_0\to S_p$ and $\sigma'^{\mu}\to(\sigma'-\sigma'_0)^{\mu}$, Equation (5) may be rewritten to satisfy the axial strain-effective stress relationship with respect to the swell-compression testing conditions:

$$\varepsilon_a(\sigma') = S_p - \frac{(\sigma' - \sigma_0')^{\mu}}{\alpha_c + \beta_c(\sigma' - \sigma_0')^{\mu}}$$
$$\text{Boundary conditions}: \begin{cases} \varepsilon_a(\sigma_0') = S_p \\ \lim\limits_{\sigma' \to \infty} \left[\varepsilon_a(\sigma')\right] \cong S_p - \dfrac{1}{\beta_c} \end{cases} \tag{6}$$

Where S_p is swelling potential, which could be fixed as S_p=1/β_s (%), and σ'_0 is the nominal overburden stress at which the sample was allowed to swell (σ'_0=1kPa for this study).

The swelling pressure P_s, by definition (i.e. $\varepsilon_a(\sigma')$=0), can be expressed as:

$$P_s = \sigma_0' + \left[\frac{\alpha_c}{\beta_s - \beta_c}\right]^{\frac{1}{\mu}} \tag{7}$$

Fitting parameters in respect to the proposed swell-compression model (Equations 4 and 6) were obtained by the non-linear least-squares optimization technique. The regression accuracy was examined adopting the coefficient of determination R^2 and the normalized root mean square error *NRMSE*. Fig. 9 presents a typical illustration of the proposed swell-compression model for natural soil and the sample reinforced with fiber B where f_{AR}=30/7. Summary of the regression analysis outputs are provided in Table 6. The high R^2 and low *NRMSE* values imply an excellent agreement between actual and predicted data, both in terms of correlation and error. The R^2 values were mainly above the 0.99 margin, indicating that approximately 99% of the variations in experimental observations are captured and further explained by the proposed model. The *NRMSE* values were observed to be less than 5% for all cases, indicating a maximum prediction offset of 5% associated with the proposed swell-compression model. The fitting parameters in respect to the proposed swell-compression model are fiber-dependent. As such, a further systematic investigation into the fitting parameters may facilitate the development of empirical or dimensional relationships as a function of fiber properties, e.g. β_c=F(f_c, f_{AR}, f_{TS}). Such a framework would not only complement computational analyses but may also prove useful for numerical implementations concerning fiber-reinforced expansive soils.

5. Conclusions

The efficiency of two types of tape-shaped synthetic fibers in counteracting the soil heave upon wetting and collapse upon stressing was investigated through a series of experimental tests. Based on test results, the following points can be drawn:

- The fiber inclusions prompted a significant reduction in swelling behavior, i.e. swelling potential S_p and swelling pressure P_s. For a given type of fiber, the reduction was dependent on the fiber content f_c and the fiber aspect ratio f_{AR}, with the former taking on a more pronounced role. Meanwhile, increase in fiber width f_w led to further reduction of S_p and P_s.
- Fiber-reinforced samples exhibited an *S*-shaped swell path, suggesting three swell phases, i.e. initial, primary and secondary swelling. Variables obtained from the *S*-shaped curve were content- and aspect ratio-dependent. Completion time of the initial and primary swelling phases varied in a way opposite to that

of swelling potential S_p, while variations observed for the primary and secondary swelling rates were in direct agreement with S_p.

- The compression path for fiber-reinforced samples suggested two compression phases, i.e. elastic and plastic compression. The yield stress and the compression index were also content- and aspect ratio-dependent, with f_c=0.5% suggesting an optimal case among the tested scenarios.
- The hyperbola concept was extended to the swell-compression framework, promoting simple equations capable of simulating the swell-compression behavior of the fiber-reinforced expansive soil with an acceptable degree of accuracy.

References

Abdi, M.R., Parsapajouh, A., Arjomand, M.A., 2008. Effects of random fiber inclusion on consolidation, hydraulic conductivity, swelling, shrinkage limit and desiccation cracking of clays. Int. J. Civ. Eng. 6, 284–292.

Al-Akhras, N.M., Attom, M.F., Al-Akhras, K.M., Malkawi, A.I.H., 2008. Influence of fibers on swelling properties of clayey soil. Geosynth. Int. 15, 304–309. doi:10.1680/gein.2008.15.4.304

Al-Rawas, A.A., Hago, A.W., Al-Sarmi, H., 2005. Effect of lime, cement and Sarooj (artificial pozzolan) on the swelling potential of an expansive soil from Oman. Build. Environ. 40, 681–687. doi:10.1016/j.buildenv.2004.08.028

Attom, M.F., Al-Akhras, N.M., Malkawi, A.I.H., 2009. Effect of fibres on the mechanical properties of clayey soil. Proc. ICE - Geotech. Eng. 162, 277–282. doi:10.1680/geng.2009.162.5.277

Boone, S.J., 2010. A critical reappraisal of “preconsolidation pressure” interpretations using the oedometer test. Can. Geotech. J. 47, 281–296. doi:10.1139/T09-093

Cai, Y., Shi, B., Ng, C.W.W., Tang, C.S., 2006. Effect of polypropylene fibre and lime admixture on engineering properties of clayey soil. Eng. Geol. 87, 230–240. doi:10.1016/j.enggeo.2006.07.007

Casagrande, A., 1936. The determination of pre-consolidation load and its practical significance, in: Casagrande, A., Rutledge, P.C., Watson, J.D. (Eds.), 1st International Conference on Soil Mechanics and Foundation Engineering. ASCE, Cambridge, Massachusetts, pp. 60–64.

Chaduvula, U., Viswanadham, B.V.S., Kodikara, J., 2017. A study on desiccation cracking behavior of polyester fiber-reinforced expansive clay. Appl. Clay Sci. in press, 1–10. doi:10.1016/j.clay.2017.02.008

Chen, Y.G., Jia, L.Y., Li, Q., W. M., Y., Cui, Y.J., Chen, B., 2017. Swelling deformation of compacted GMZ bentonite experiencing chemical cycles of sodium-calcium exchange and salinization-desalinization effect. Appl. Clay Sci. 141, 55–63. doi:10.1016/j.clay.2017.02.016

Chong, S., Santamarina, J.C., 2016. Soil compressibility models for a wide stress range. J. Geotech. Geoenvironmental Eng. 142, 6016003–7. doi:10.1061/(ASCE)GT.1943-5606.0001482

Consoli, N.C., Vendruscolo, M.A., Fonini, A., Rosa, F.D., 2009. Fiber reinforcement effects on sand considering a wide cementation range. Geotext. Geomembranes 27, 196–203. doi:10.1016/j.geotexmem.2008.11.005

Cui, S.L., Zhang, H.Y., Zhang, M., 2012. Swelling characteristics of compacted GMZ bentonite-sand mixtures as a buffer/backfill material in China. Eng. Geol. 141–142, 65–73. doi:10.1016/j.enggeo.2012.05.004

Cui, Y.J., Delage, P., 1996. Yielding and plastic behaviour of an unsaturated compacted silt. Géotechnique 46, 291–311. doi:10.1680/geot.1996.46.2.291

Dakshanamurthy, V., 1978. A new method to predict swelling using hyperbola equation. Geotech. Eng. J. SEAGS AGSSEA 8, 29–38.

Estabragh, A.R., Bordbar, A.T., Javadi, A.A., 2011. Mechanical behavior of a clay soil reinforced with nylon fibers. Geotech. Geol. Eng. 29, 899–908. doi:10.1007/s10706-011-9427-8

Estabragh, A.R., Namdar, P., Javadi, A.A., 2012. Behavior of cement-stabilized clay reinforced with nylon fiber. Geosynth. Int. 19, 85–92. doi:10.1680/gein.2012.19.1.85

Estabragh, A.R., Rafatjo, H., Javadi, A.A., 2014. Treatment of an expansive soil by mechanical and chemical techniques. Geosynth. Int. 21, 233–243. doi:10.1680/gein.14.00011

Estabragh, A.R., Soltani, A., Javadi, A.A., 2016. Models for predicting the seepage velocity and seepage force in a fiber reinforced silty soil. Comput. Geotech. 75, 174–181. doi:10.1016/j.compgeo.2016.02.002

Kalkan, E., 2011. Impact of wetting–drying cycles on swelling behavior of clayey soils modified by silica fume. Appl. Clay Sci. 52, 345–352. doi:10.1016/j.clay.2011.03.014

Kalkan, E., 2013. Preparation of scrap tire rubber fiber–silica fume mixtures for modification of clayey soils. Appl. Clay Sci. 80–81, 117–125. doi:10.1016/j.clay.2013.06.014

Kumar, A., Walia, B.S., Bajaj, A., 2007. Influence of fly Ash, lime, and polyester fibers on compaction and strength properties of expansive soil. J. Mater. Civ. Eng. 19, 242–248. doi:10.1061/(ASCE)0899-1561(2007)19:3(242)

Mirzababaei, M., Miraftab, M., Mohamed, M., McMahon, P., 2013. Impact of carpet waste fibre addition on swelling properties of compacted clays. Geotech. Geol. Eng. 31, 173–182. doi:10.1007/s10706-012-9578-2

Mirzababaei, M., Yasrobi, S.S., Al-Rawas, A.A., 2009. Effect of polymers on swelling potential of expansive soils. Proc. ICE - Gr. Improv. 162, 111–119. doi:10.1680/grim.2009.162.3.111

Nalbantoglu, Z., 2006. Lime stabilization of expansive clay, in: Al-Rawas, A.A., Goosen, M.F.A. (Eds.), Expansive Soils: Recent Advances in Characterization and Treatment. Taylor & Francis Group, London, pp. 341–348. doi:10.1201/9780203968079.ch23

Phanikumar, B.R., Singla, R., 2016. Swell-consolidation characteristics of fibre-reinforced expansive soils. Soils Found. 56, 138–143. doi:10.1016/j.sandf.2016.01.011

Plé, O., Lê, T.N.H., 2012. Effect of polypropylene fiber-reinforcement on the mechanical behavior of silty clay. Geotext. Geomembranes 32, 111–116. doi:10.1016/j.geotexmem.2011.11.004

Punthutaecha, K., Puppala, A.J., Vanapalli, S.K., Inyang, H., 2006. Volume change behaviors of expansive soils stabilized with recycled ashes and fibers. J. Mater. Civ. Eng. 18, 295–306. doi:10.1061/(ASCE)0899-1561(2006)18:2(295)

Puppala, A.J., Musenda, C., 2000. Effects of fiber reinforcement on strength and volume change in expansive soils. Transp. Res. Rec. J. Transp. Res. Board 1736, 134–140. doi:10.3141/1736-17

Rao, S.M., Thyagaraj, T., Thomas, H.R., 2006. Swelling of compacted clay under osmotic gradients. Géotechnique 56, 707–713. doi:10.1680/geot.2006.56.10.707

Shahbazi, M., Rowshanzamir, M., Abtahi, S.M., Hejazi, S.M., 2016. Optimization of carpet waste fibers and steel slag particles to reinforce expansive soil using response surface methodology. Appl. Clay Sci. in press, 1–8. doi:10.1016/j.clay.2016.11.027

Sivakumar Babu, G.L., Vasudevan, A.K., Sayida, M.K., 2008. Use of coir fibers for improving the engineering properties of expansive soils. J. Nat. Fibers 5, 61–75. doi:10.1080/15440470801901522

Sivapullaiah, P. V., Sridharan, A., Stalin, V.K., 1996. Swelling behaviour of soil-bentonite mixtures. Can. Geotech. J. 33, 808–814. doi:10.1139/t96-106-326

Soltani, A., 2016. Discussion of "Compressibility behavior of soils: A statistical approach" by Syed Iftekhar Ahmed and Sumi Siddiqua [Geotechnical and Geological Engineering, doi: 10.1007/s10706-016-9996-7]. Geotech. Geol. Eng. 34, 1687–1692. doi:10.1007/s10706-016-0062-2

Soltani, A., Taheri, A., Khatibi, M., Estabragh, A.R., 2017. Swelling potential of a stabilized expansive soil: A comparative experimental study. Geotech. Geol. Eng. in press, 1–28. doi:10.1007/s10706-017-0204-1

Sridharan, A., Gurtug, Y., 2005. Compressibility characteristics of soils. Geotech. Geol. Eng. 23, 615–634. doi:10.1007/s10706-004-9112-2

Sridharan, A., Gurtug, Y., 2004. Swelling behaviour of compacted fine-grained soils. Eng. Geol. 72, 9–18. doi:10.1016/S0013-7952(03)00161-3

Sridharan, A., Prakash, K., 2000. Classification procedures for expansive soils. Proc. ICE - Geotech. Eng. 143, 235–240. doi:10.1680/geng.2000.143.4.235

Sridharan, A., Rao, A., Sivapullaiah, P., 1986. Swelling pressure of clays. Geotech. Test. J. 9, 24–33. doi:10.1520/GTJ10608J

Tang, C.S., Shi, B., Zhao, L.Z., 2010. Interfacial shear strength of fiber reinforced soil. Geotext. Geomembranes 28, 54–62. doi:10.1016/j.geotexmem.2009.10.001

Tang, C., Shi, B., Gao, W., Chen, F., Cai, Y., 2007. Strength and mechanical behavior of short polypropylene fiber reinforced and cement stabilized clayey soil. Geotext. Geomembranes 25, 194–202. doi:10.1016/j.geotexmem.2006.11.002

Trouzine, H., Bekhiti, M., Asroun, A., 2012. Effects of scrap tyre rubber fibre on swelling behaviour of two clayey soils in Algeria. Geosynth. Int. 19, 124–132. doi:10.1680/gein.2012.19.2.124

Viswanadham, B.V.S., Phanikumar, B.R., Mukherjee, R. V., 2009. Swelling behaviour of a geofiber-reinforced expansive soil. Geotext. Geomembranes 27, 73–76. doi:10.1016/j.geotexmem.2008.06.002

Viswanadham, B.V.S., Phanikumar, B.R., Mukherjee, R. V., 2009. Effect of polypropylene tape fibre reinforcement on swelling behaviour of an expansive soil. Geosynth. Int. 16, 393–401. doi:10.1680/gein.2009.16.5.393

Yazdandoust, F., Yasrobi, S.S., 2010. Effect of cyclic wetting and drying on swelling behavior of polymer-stabilized expansive clays. Appl. Clay Sci. 50, 461–468. doi:10.1016/j.clay.2010.09.006

Ye, W.M., Zhu, C.M., Chen, Y.G., Chen, B., Cui, Y.J., Wang, J., 2015. Influence of salt solutions on the swelling behavior of the compacted GMZ01 bentonite. Environ. Earth Sci. 74, 793–802. doi:10.1007/s12665-015-4108-1

List of Tables

Table 1 – A summary of some of the more recent contributions addressing the aspect ratio-dependent swelling phenomenon

Reference	**Type of fiber**	**Shape of fiber**	**Content** f_c **(%)**	**Length** f_l **(mm)**	**Diameter or width** f_d **or** f_w **(mm)**	**Aspect ratio** $f_{AR}=f_l/f_d$ **or** f_w
Abdi et al. (2008)	Polypropylene	Bar-shaped	1 2 4 8	5 10 15	N/A	N/A
Al-Akhras et al. (2008)	Nylon	Bar-shaped	1 2 3 4 5	5 10 15 20	0.2	25 50 75 100
	Palmyra fiber	Bar-shaped		10 20 30 40	0.4	
Sivakumar Babu et al. (2008)	Coir fiber	Bar-shaped	1.0 1.5 2.0 2.5	15	0.25 0.35	60 ≈43
Viswanadham et al. (2009[a, b])	Polypropylene	Tape-shaped	0.25 0.50	30 60 90	2	15 30 45
Estabragh et al. (2014)	Polyethylene	Bar-shaped	0.5 1.0 1.5	10 20 30	0.3	≈33 ≈67 100
	Polypropylene	Tape-shaped			3.0	≈3 ≈7 10
	Polypropylene	Tape-shaped			5.0	2 4 6
Phanikumar and Singla (2016)	Nylon	Bar-shaped	0.05 0.10 0.15 0.20 0.25 0.30	15 20	1	15 20
Shahbazi et al. (2016)	Polyacrylonitrile	Bar-shaped	0.2 0.9 1.6 2.3 3.0	N/A	N/A	5 15 25 35 45

Table 2 – Mechanical properties of the expansive soil

Properties	**Standard designation**	**Value**
Specific gravity, G_s	ASTM D854	2.76
Clay (<2μm) (%)		41.15
Silt (2–75μm) (%)	ASTM D422-63	42.75
Sand (0.075–4.75mm) (%)		16.10
Liquid limit, *LL* (%)		85.30
Plastic limit, *PL* (%)	ASTM D4318	26.05
Plasticity index, *PI* (%)		59.25
Shrinkage limit, *SL* (%)	ASTM D427	10.34
USCS Classification	ASTM D2487	CH
Swelling potential, S_p^{1kPa} (%)		26.40
Swelling potential, S_p^{7kPa} (%)	ASTM D4546	17.50
Swelling pressure, P_s (kPa)		325
Maximum dry unit weight, $\gamma_{d\max}$ (kN/m^3)	ASTM D698	14.95
Optimum moisture content, ω_{opt} (%)		23.40

Notes:
$\boldsymbol{S_p^{1kpa}}$ = % Expansion from optimum moisture content under σ'_0=1kPa
$\boldsymbol{S_p^{7kpa}}$ = % Expansion from air-dry condition under σ'_0=7kPa

Table 3 – Physical and mechanical properties of the fibers (as supplied by the manufacturer)

Type of fiber	**Fiber A**	**Fiber B**
Properties	**Value**	
Specific gravity, G_s	0.72	0.85
Width, f_w (mm)	2.5	7.0
Thickness, f_t (mm)	0.01	0.03
Tensile strength, f_{TS} (MPa)	1250	3000
Young's modulus, f_E (MPa)	7000	5000
Type	Single fiber	
Shape	Tape-shaped	
Water adsorption	Negligible	
Resistance to acid and alkaline	Excellent	

Table 4 – Mechanical properties of the prepared samples

Fiber	f_c (%)	$f_{AR}=f_l/f_w$	ω_{opt} (%)	γ_{dmax} (kN/m^3)	e_0
–	–	–	23.40	14.95	0.811
Fiber A	0.5	15/2.5	22.35	14.80	0.823
	1.0		22.10	14.62	0.838
	1.5		21.72	14.30	0.872
	0.5	30/2.5	25.15	14.50	0.860
	1.0		23.45	14.50	0.853
	1.5		21.05	13.92	0.924
Fiber B	0.5	15/7	22.20	14.40	0.874
	1.0		21.95	14.12	0.904
	1.5		21.20	13.96	0.919
	0.5	30/7	22.22	14.25	0.893
	1.0		25.11	14.15	0.900
	1.5		26.15	13.60	0.970

Table 5 – Summary of the swell-time and compressibility curve variables for the tested samples

Fiber	f_c (%)	$f_{AR}=f_l/f_w$	t_{is} (min)	t_{ps} (min)	ε_{ais} (%)	ε_{aps} (%)	ε_{ass} (%)	S_p (%)	C_{ps}	C_{ss}	P_s (kPa)	C_c	σ_y (kPa)
–	–	–	45	1640	3.71	19.22	3.47	26.40	1.23×10^{-1}	3.87×10^{-2}	325	0.388	45
Fiber A	0.5	15/2.5	110	3750	2.67	18.37	1.91	22.95	1.20×10^{-1}	3.55×10^{-2}	215	0.331	38
	1.0		115	4200	2.25	18.22	1.58	22.05	1.17×10^{-1}	3.23×10^{-2}	198	0.388	49
	1.5		155	4450	2.48	15.97	1.40	19.85	1.10×10^{-1}	3.02×10^{-2}	177	0.405	82
	0.5	30/2.5	130	4200	2.84	17.90	1.71	22.45	1.19×10^{-1}	3.49×10^{-2}	205	0.377	44
	1.0		160	4460	2.48	15.45	1.37	19.30	1.07×10^{-1}	2.96×10^{-2}	192	0.401	55
	1.5		265	6100	2.10	13.05	0.85	16.00	9.58×10^{-2}	2.60×10^{-2}	135	0.443	66
Fiber B	0.5	15/7	155	4255	2.27	16.20	1.63	20.10	1.13×10^{-1}	3.37×10^{-2}	201	0.340	38
	1.0		165	4625	2.38	14.47	1.35	18.20	1.00×10^{-1}	3.02×10^{-2}	163	0.386	41
	1.5		200	5110	2.16	13.09	1.10	16.35	9.30×10^{-2}	2.72×10^{-2}	136	0.431	76
	0.5	30/7	140	4510	2.57	16.51	1.47	20.55	1.09×10^{-1}	3.21×10^{-2}	158	0.382	39
	1.0		170	4710	2.19	12.82	1.19	16.20	8.89×10^{-2}	2.71×10^{-2}	124	0.390	42
	1.5		190	5765	1.78	9.67	0.70	12.15	6.52×10^{-2}	1.99×10^{-2}	97	0.461	53

Table 6 – Summary of the regression analysis outputs in respect to the proposed swell-compression model (Equations 4, 6 and 7)

Fiber	f_c (%)	$f_{AR}=f_l/f_w$	α_s	β_s	R^2	*NRMSE* (%)	S_p (%)	$1/\beta_s$ (%)	$\varepsilon_a(t_{ss})$ (%)	α_c	β_c	μ	R^2	*NRMSE* (%)	P_s^a (kPa)	P_s^m (kPa)
–	–	–	10.79	3.73×10^{-2}	0.994	3.3	26.40	26.81	26.22	0.951	1.68×10^{-2}	0.661	0.999	0.9	325	335
Fiber A	0.5	15/2.5	34.59	4.01×10^{-2}	0.993	3.5	22.95	24.94	23.38	0.318	1.20×10^{-2}	0.453	0.992	3.1	215	214
	1.0		42.24	4.09×10^{-2}	0.990	4.2	22.05	24.45	22.65	0.293	3.72×10^{-3}	0.389	0.994	2.9	198	204
	1.5		51.80	4.52×10^{-2}	0.990	4.1	19.85	22.12	20.33	0.303	1.35×10^{-3}	0.377	0.993	3.1	177	169
	0.5	30/2.5	41.37	4.11×10^{-2}	0.991	4.0	22.45	24.33	22.58	0.321	8.17×10^{-3}	0.433	0.996	2.4	205	194
	1.0		54.25	4.71×10^{-2}	0.995	3.0	19.30	21.23	19.50	0.372	4.86×10^{-3}	0.418	0.993	3.1	192	183
	1.5		103.84	5.33×10^{-2}	0.994	3.1	16.00	18.76	16.31	0.354	1.26×10^{-3}	0.396	0.989	3.7	135	127
Fiber B	0.5	15/7	53.30	4.43×10^{-2}	0.995	3.2	20.10	22.57	20.66	0.582	1.76×10^{-2}	0.589	0.990	3.9	201	188
	1.0		60.54	4.95×10^{-2}	0.995	2.9	18.20	20.20	18.46	0.742	1.67×10^{-2}	0.625	0.995	2.7	163	149
	1.5		79.13	5.47×10^{-2}	0.996	2.8	16.35	18.28	16.45	0.355	1.92×10^{-4}	0.388	0.994	2.7	136	126
	0.5	30/7	48.74	4.36×10^{-2}	0.995	3.2	20.55	22.94	21.11	0.387	1.32×10^{-2}	0.505	0.994	3.1	158	156
	1.0		70.68	5.61×10^{-2}	0.992	3.8	16.20	17.83	16.25	1.012	1.85×10^{-2}	0.689	0.996	2.5	124	120
	1.5		109.18	7.25×10^{-2}	0.987	4.8	12.15	13.79	12.36	1.849	1.85×10^{-2}	0.785	0.995	2.6	97	91

Notes:
$1/\beta_s$ = Long-term predicted swelling potential
$\varepsilon_a(t_{ss})$ = Short-term predicted swelling potential (Equation 4 when t=t_{ss}=216hr)
P_s^a = Actual swelling pressure
P_s^m = Predicted swelling pressure (Equation 7)

List of Figures

Fig. 1 – Loose tape-shaped polypropylene fibers

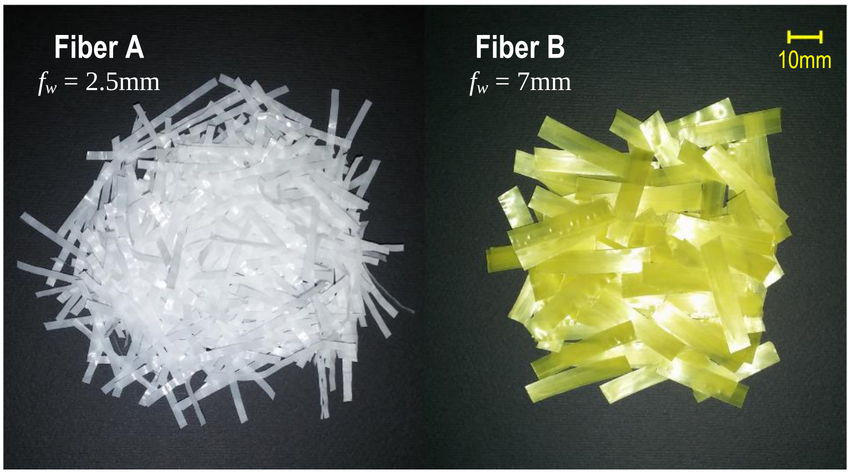

Fig. 2 – Axial strain-time curves for natural soil and samples reinforced with fiber A: **(a)** f_{AR}=15/2.5; **(b)** f_{AR}=30/2.5

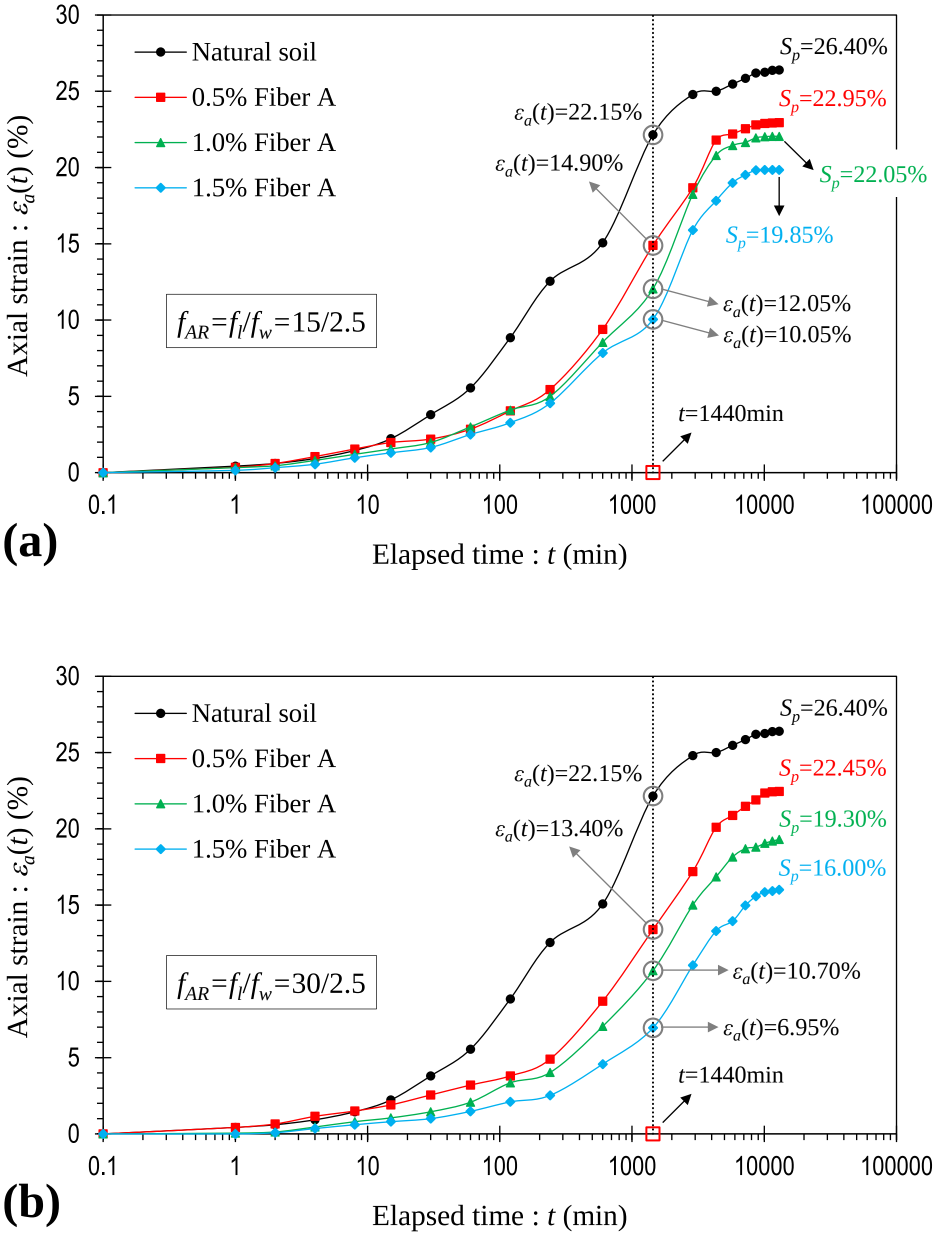

Fig. 3 – Axial strain-time curves for natural soil and samples reinforced with fiber B: **(a)** f_{AR}=15/7; **(b)** f_{AR}=30/7

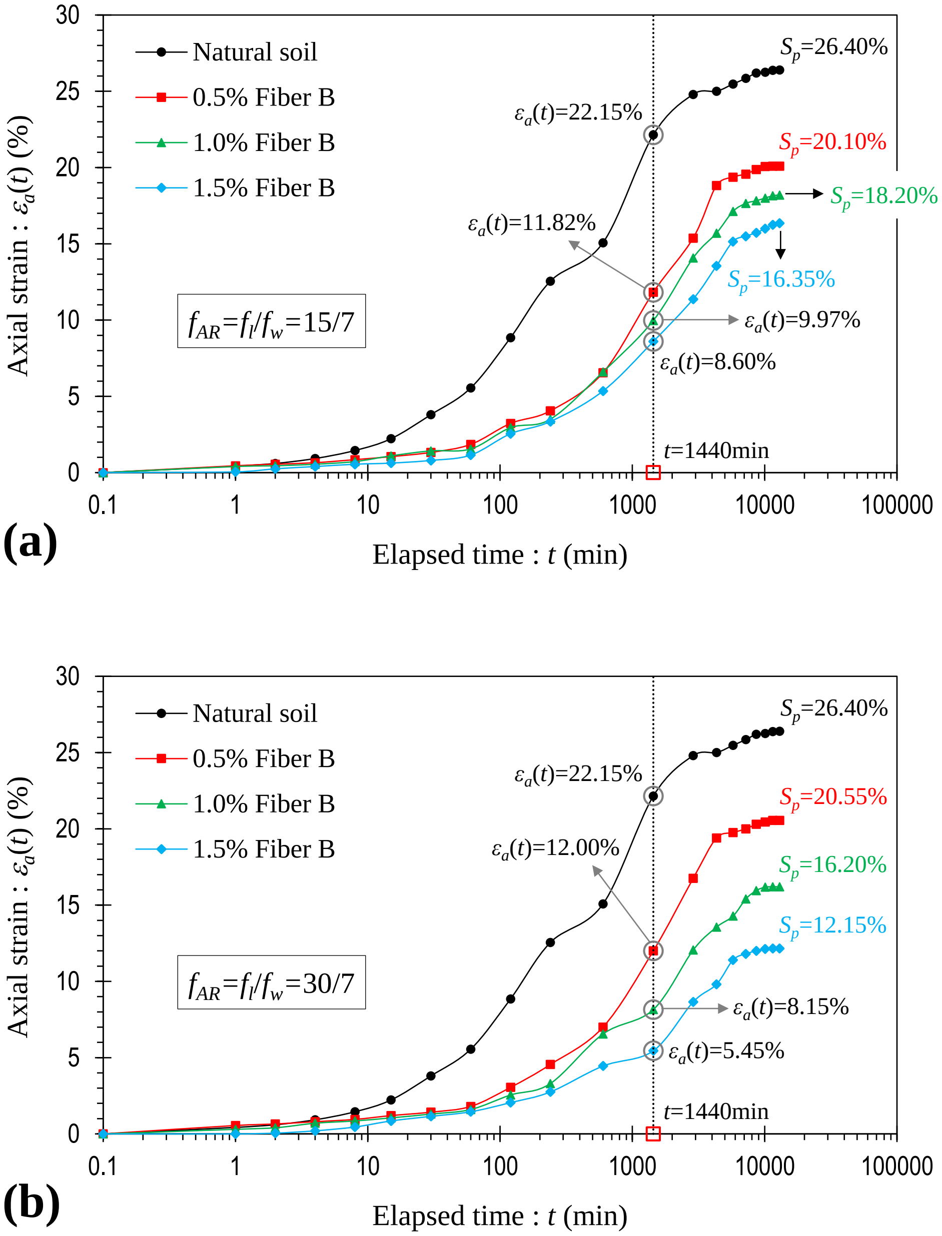

Fig. 4 – Axial strain-effective stress curves for natural soil and samples reinforced with fiber A: **(a)** f_{AR}=15/2.5; **(b)** f_{AR}=30/2.5

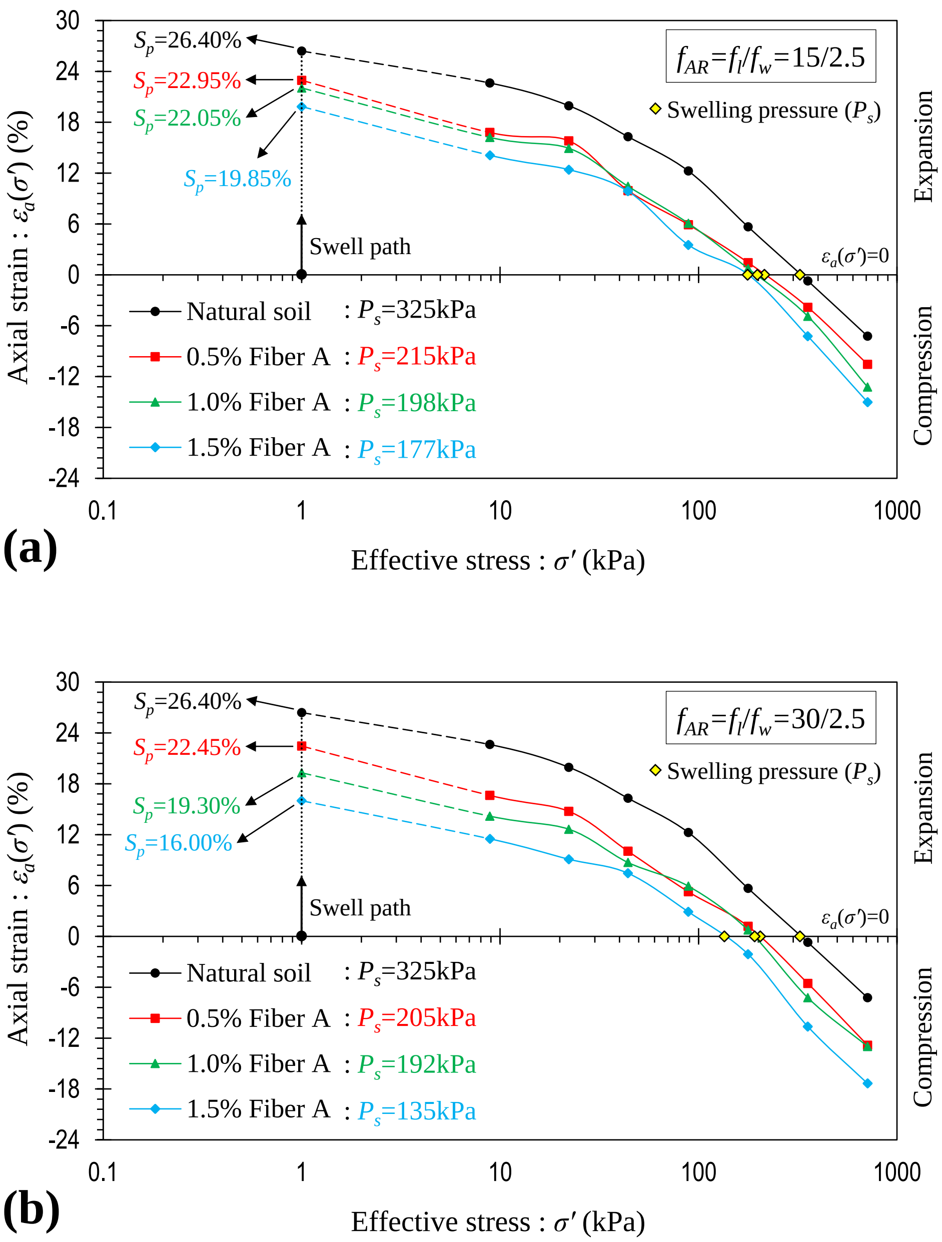

Fig. 5 – Axial strain-effective stress curves for natural soil and samples reinforced with fiber B: **(a)** f_{AR}=15/7; **(b)** f_{AR}=30/7

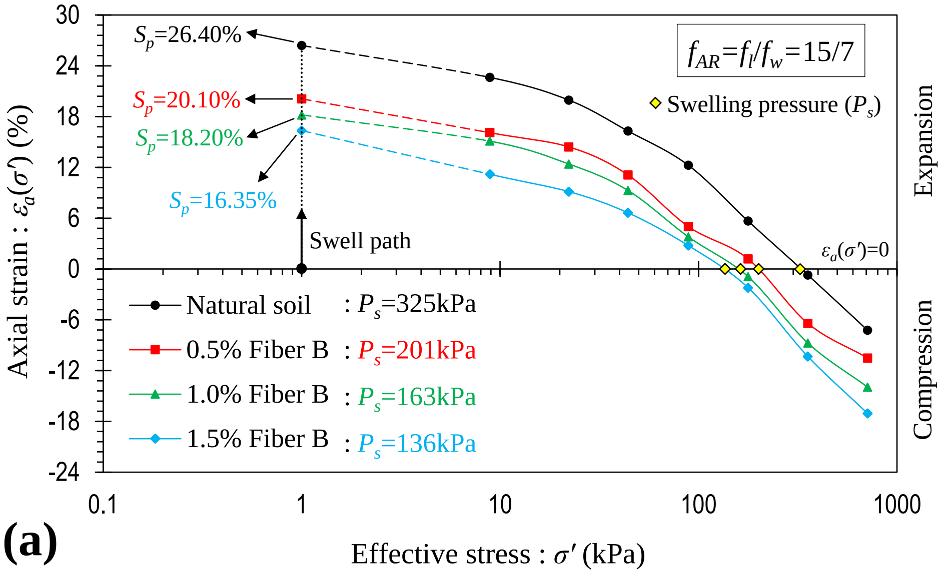

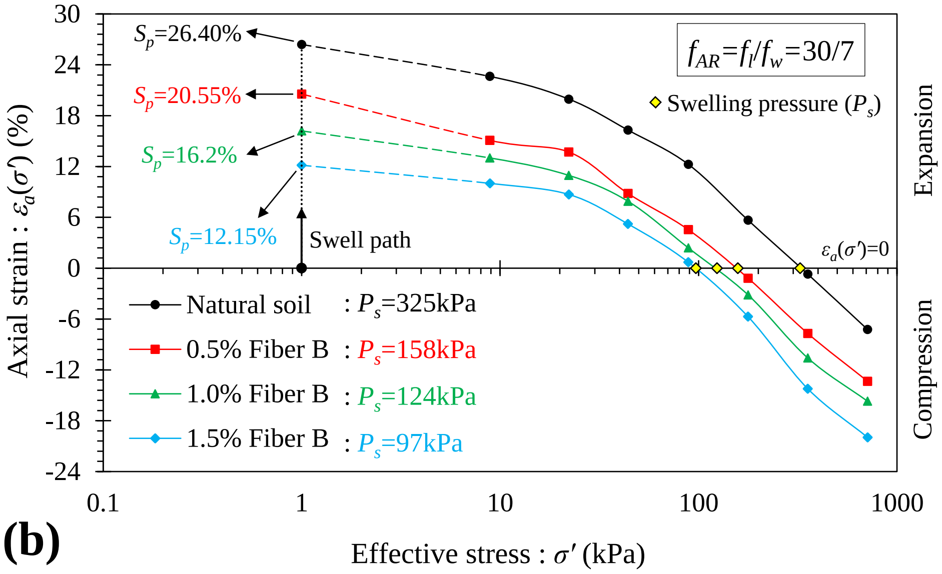

Fig. 6 – Variations of **(a)** S_p and **(b)** P_s against fiber content for the tested samples

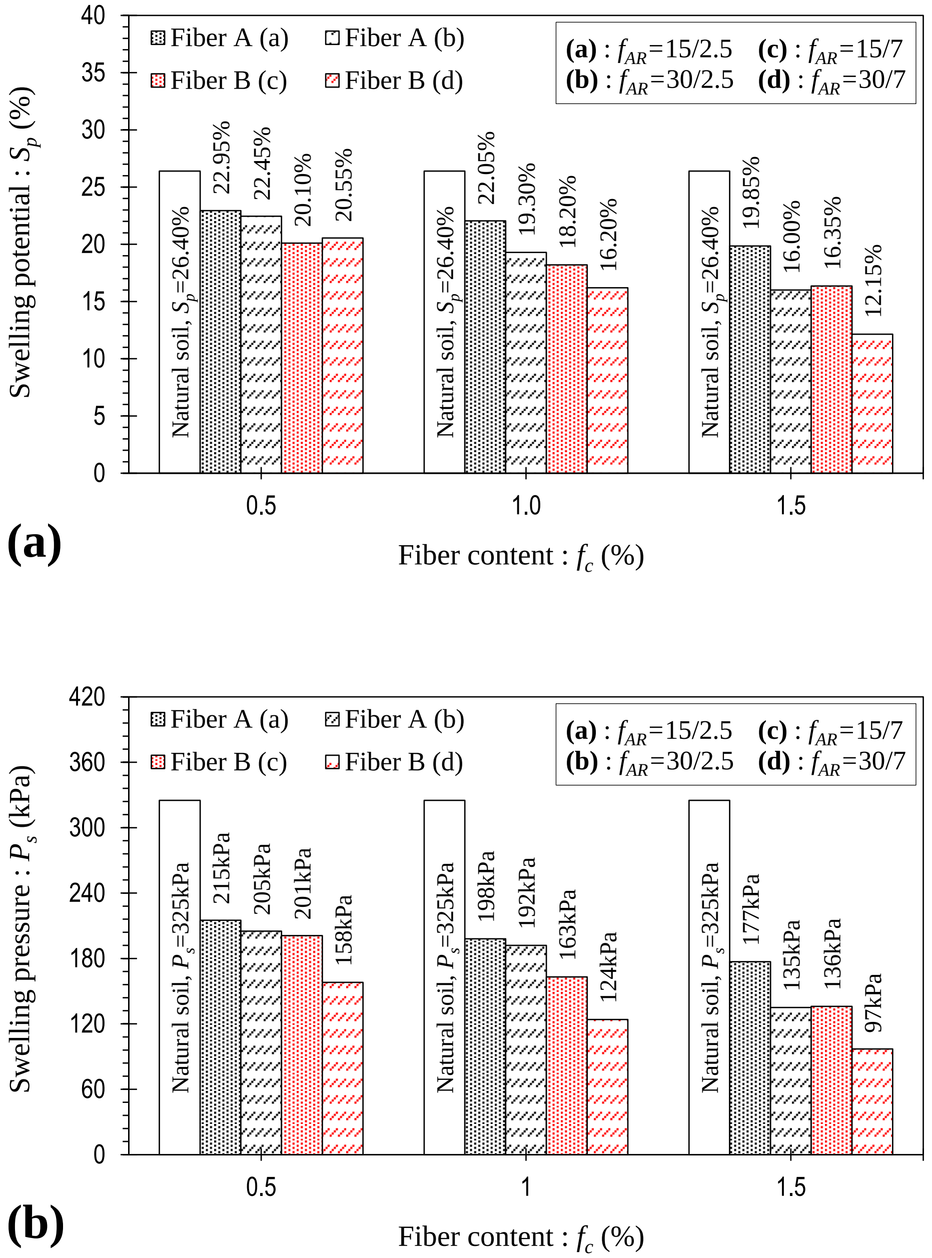

Fig. 7 – **(a)** Axial strain-time (swell) and **(b)** axial strain-effective stress (compression) characteristics

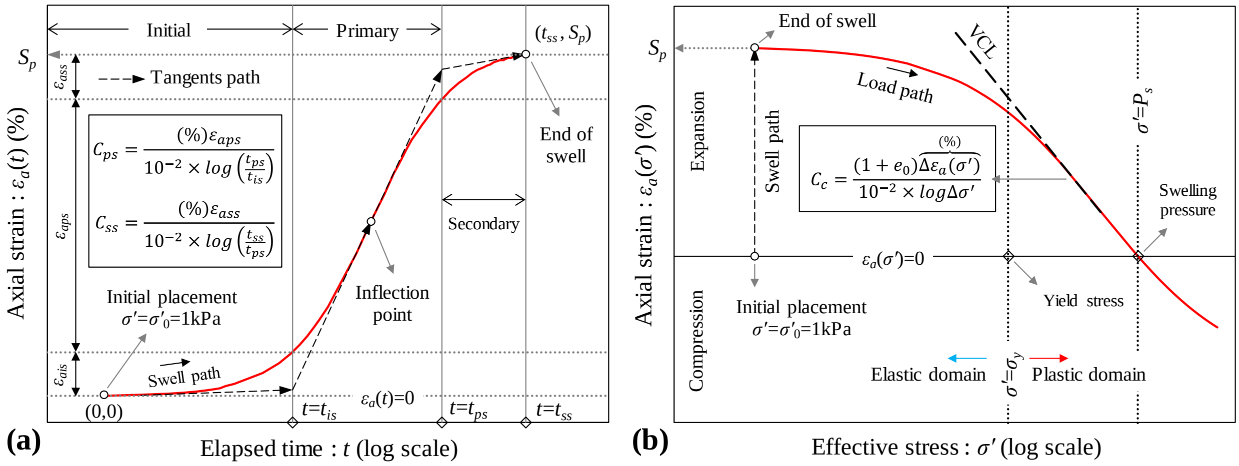

Fig. 8 – Variations of **(a)** C_{ps} and **(b)** C_{ss} against fiber content for the tested samples

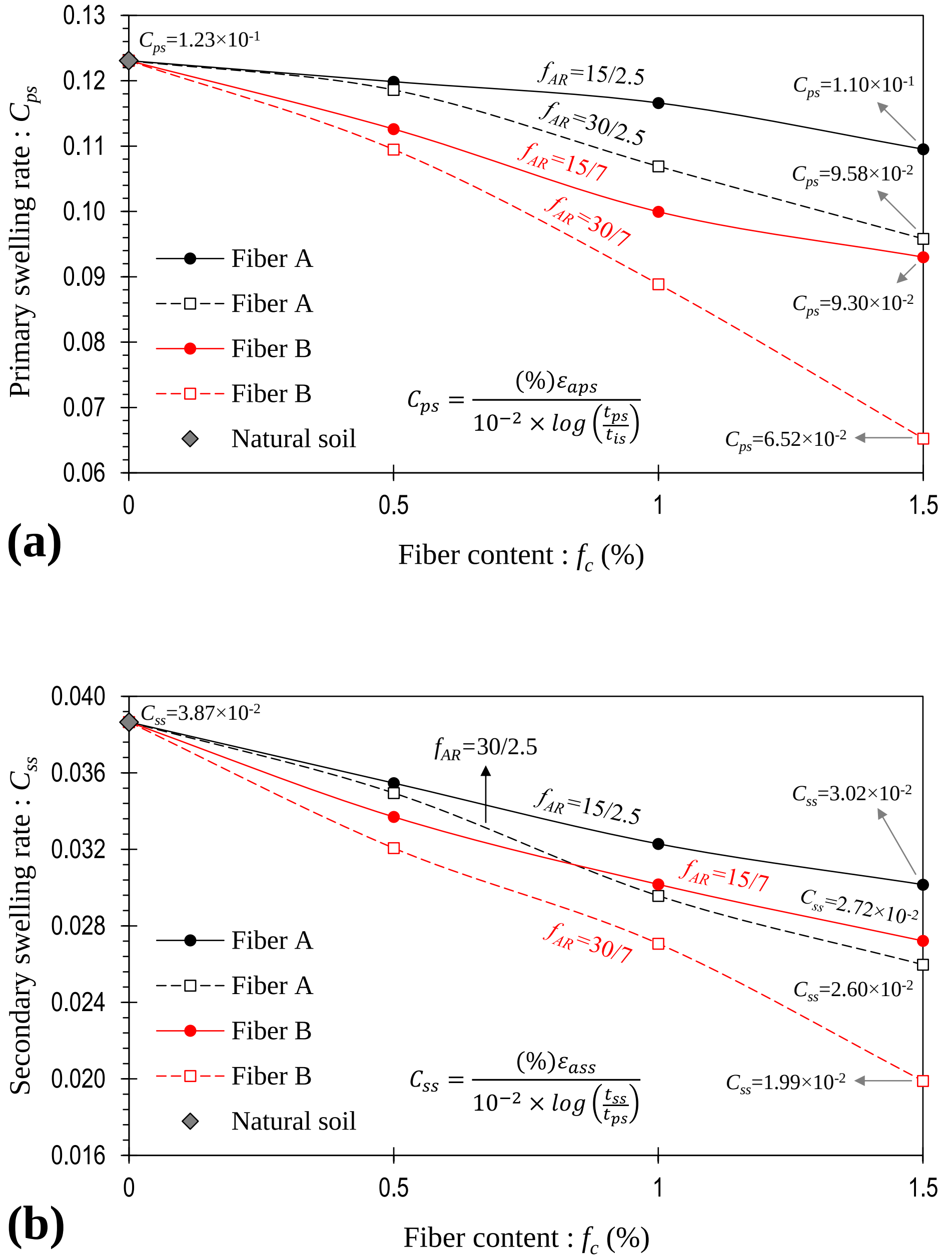

Fig. 9 – Typical illustration of the proposed swell-compression model (Equations 4, 6 and 7) for natural soil and samples reinforced with fiber B where f_{AR}=30/7